

## Structure of Northeastern Sakurajima, South Kyushu, Japan, Revealed by Seismic Reflection Survey

Tomoki TSUTSUI\*, Naofumi YAGI\*\*, Masato IGUCHI\*\*\*, Takeshi TAMEGURI\*\*\*\*,  
Hitoshi MIKADA\*\*\*\*\*, Kyosuke ONISHI\*\*\*\*\*, (present \*), Hiroki MIYAMACHI\*\*\*\*\*,  
Takeshi NISHIMURA\*\*\*\*\*, Yuichi MORITA\*\*\*\*\* and Atsushi WATANABE\*\*\*\*\*

(Received June 27, 2011; Accepted September 3, 2012)

Seismic reflection structure in the northeast part of Sakurajima Volcano is discussed down to ca. 11 km with three profiles. Data acquisition was conducted along intersecting two lines with 221 stations and eight shot points. The two lines covered the northeastern portion of the volcano. One of the lines was spread along NNW to SSE direction in the east foot, and another line was oriented east to west in the northern flank of the volcano. Data processing were made through the conventional procedure of the reflection seismology, and depth migrated sections were obtained. Four continuous reflection horizons appear in the profiles. One of the reflection horizons around 5.4 km depth disappears in the northeast portion of the coverage area. The interruption of the horizon suggests existence of magma or magma supply path beneath it. The inferred magma supply path locates to the west of that previously presented.

**Key words:** Sakurajima volcano, Seismic structure, Seismic exploration

### 1. Introduction

Sakurajima is an active volcano with an altitude of 1117 m located in southern Kyushu. In Sakurajima volcano, effusive eruptions were recorded in history (Fukuyama and Kobayashi, 1981). In this half century, frequent explosions from the summit crater of Mt. Minamidake begun in 1955 and continued afterwards until 1990's. Recently, the Showa crater opened again at the eastern flank of the Mt. Minamidake in June 2006, and explosive eruptions from the crater have been enhanced since February 2008 (Iguchi *et al.* 2008).

Such progress of the activity has a close relation to accumulation of the magma in the reservoir beneath Aira caldera in the depth of 10 km, and movement of the magma to the deep part below Mt. Minamidake. According to ground deformation analyses, two pressure sources are presented in the depth of 10 km beneath Aira caldera, and at 5 km depth beneath Mt. Minamidake and are inferred as magma chambers. For example, Eto *et al.* (1997) explained that subsiding ground deformation during 1974–1992 is due to the major pressure source in the depth of 10 km beneath Aira caldera and the additional pressure source

beneath Mt. Minamidake. Hidayati *et al.* (2007) presented a model that magma moves along a tensile crack from northeast to the southwest through the foot of Mt. Minamidake, which was inferred from inflation around Aira caldera and the seismicity in northeastern Sakurajima (Fig. 1).

The subsurface structure of Sakurajima volcano has been investigated by gravity survey and by electromagnetic sounding. Yokoyama and Ohkawa (1986) constructed the first density model and presented the gravity basement depth at 2.5 km beneath Sakurajima volcano and a graben-like structure beneath Kagoshima Bay from the Bouguer anomaly. Then Komazawa *et al.* (2008) performed the high density gravity survey, and presented detailed topography of the gravity basement around 1.2 km b. s. l., which is approximately northeastern dip and ridges eastward in the northeast Sakurajima. Furthermore, Kanda *et al.* (2008) performed the AMT electromagnetic sounding in Sakurajima, and revealed that a high resistivity layer is deeper in northeastern part than in other part in Sakurajima. The deeper high resistivity layer implies the basement and underlies the low resistivity layer which is possibly contained by permeable materials.

\* Graduate school of Resource Science and Engineering,  
Akita University.

\*\* Fujitsu Software Technologies Limited.

\*\*\* Disaster Prevention Research Institute, Kyoto University.

\*\*\*\* Graduate school of Engineering, Kyoto University.

\*\*\*\*\* Graduate school of Science and Engineering, Kagoshima

University.

\*\*\*\*\* Graduate school of Science, Tohoku University.

\*\*\*\*\* Earthquake Research Institute, University of Tokyo.

Corresponding author: Tomoki Tsutsui  
e-mail: tomoki@gipc.akita-u.ac.jp

Thus the northeastern Sakurajima is the key location in order to discuss movement of magma to Sakurajima. In the 2008 Project of Artificial Explosion Experiment at Sakurajima Volcano (Iguchi *et al.*, 2009), seismic reflection survey was carried out at the northeast portion in Sakurajima, expecting any evidence of magma supply paths. This paper discusses the underground structure from the depth of 2 km down to ca. 11 km beneath the Sakurajima volcano through the 2008's reflection survey.

## 2. Observation and data

The 2008 Project of Artificial Explosion Experiment was carried out on the Sakurajima volcano and its surroundings in November 2008 as a part of the 7th national project for prediction of volcanic eruption. Reflection survey was concentrated at east to north flank of Sakurajima. In this survey, two seismic lines which consist of 221 temporary seismic stations and eight shot points were deployed as shown in Fig. 1 (Iguchi *et al.*, 2009). The field parameters are listed in Table 1. The line NS consists of 126 stations X001A - X125A, and X192A which are deployed in the east foot of the volcano, and the line EW

consists of 95 stations X001B - X094B, and X101B which are deployed on the north flank. Average separations of stations were 47 m along the line NS and 72 m along the line EW. In each seismic station, the vertical component seismometer (natural frequency: 4.5 Hz), was installed and the seismic signal was recorded in the recorder LS-8200SD (Hakusan industry corp.) with sampling interval of 2 ms.

Along the line NS, four shot points, S09, S10, S11, and S12, are aligned from the south. As for the line EW, five shot points, S15, S14, S13, S11, and S06, are aligned from the west. The shot point S11 is located at the intersection of the lines NS and EW.

## 3. Data processing

The flow of the main analyses is presented in Fig. 2. The software package Seismic Un\*x (Cohen and Stockwell, 2008) was used for data processing, which installed in Macintosh system (Yagi and Tsutsui, 2009). Purposes and theory of each step are described in Yilmaz (2001).

In the static correction, the datum was assigned as 372 m above sea level and the static-correction velocity of 1.1 km/s is applied with referring to Tsutsui *et al.* (2011).

The sorting parameters are shown in Table. 2. Geometry of the profiles are shown in Fig. 3. CMP spacing is the half of the mean station separation in each line. The line EW was split at the shot S11 into two portions, the profiles EW(W) and EW(E) because of its bending geometry. Local coordinate systems are used along each profile, orienting x-axis to the north for the line NS or to the east in the line EW, respectively. The both origins are assigned at the shot point S11. Major analyses and the parameters are described as follows.

Fig. 4 shows examples of the shot records in the profiles NS and EW(W). Fig. 4 correspond to the labeled step <1> in Fig. 2. AGC (Automatic Gain Control) was applied on the seismograms with 0.6 s in gate time. Artificial quiescence appears before the first arrival. Parasitic later arrivals with parallel to the first arrival are dominant and likely mask deeper reflections out in the sections.

The filtered shot records are shown in Fig. 5. Fig. 5 corresponds to the labeled step <2> in Fig. 2. The arrows mark enhanced arrivals with high apparent velocity. The three-point mixing, the band-pass filtering (1–8 Hz), the

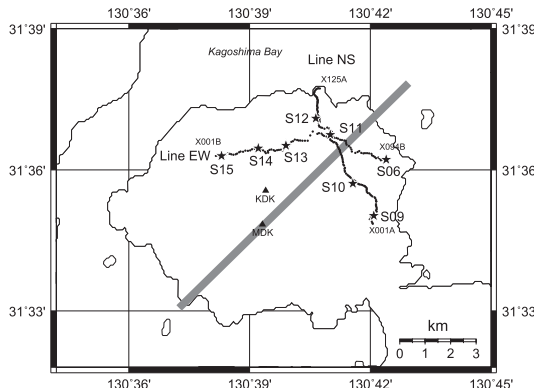


Fig. 1. Seismic lines. Stars present the shot points and solid circles are temporary seismic stations. Thick line represents the tensile crack which presented by Hidayati *et al.* (2007). The solid triangles mark major summits with the following codes, such as KDK: Kitadake, MDK: Minami-dake.

Table 1. The field parameters.

Line	Length (km)	Shots.	Number of stations	Average spacing (m)
NS	5.7	S09, S10, S11, S12	126	47
EW	6.7	S06, S11, S13, S14, S15	95	72

Energy source: Explosives (dynamite).

Charge size; 20kg (S14), 20kg×4 (S09, S10, S11, S12, S13, S15), and 200kg(S06).

predictive deconvolution have been applied on the seismograms in order. The optimum parameters were determined through the tuning; The prediction distances were ranging between 0.8 to 1.2s and the operation length was around 0.3 s, depending on each waveform. Instrumental compensation was not applied through the processing.

We used combined CMP gathers in the velocity analysis because of poor fold number for each single CMP gather. We choose eight sets of the combined gathers for the line NS, two sets for the profile EW(W), and one set for the profile EW(E) for the analysis as taking into accounts of their fold number. Fig. 6 shows an example of velocity spectra with the final velocity function. Fig. 6 corresponds to the labeled step <3> in Fig. 2. We worked on the picking with referring to the corresponding CMP gather at the points in order to take an exact peak in the spectrum. Because of the peak broadening, accuracy of velocity picking becomes poorer with increasing travel time. Though the peak width keeps within 500 m/s until 3 s of travel time, it broadens in later travel time.

The results of the velocity analysis are shown in Fig. 7. The symbols in Fig. 7a are obtained RMS P-wave velocity

through the velocity analysis. There looks no clear spatial dependence among the pick-up values so that a single velocity function is appropriate over all the profiles. The final velocity was determined from the medians of the pick-up value in the analysis down to 3.4 s, and was imported from that of Ono *et al.* (1978) at 4.8 s because of the broadening of deeper peaks. The final stacking velocity function is shown by the solid line with solid circles.

Fig. 7b shows an interval velocity with the solid line which derived from the final stacking velocity in Fig. 7a. A broken line represents the model in Osumi peninsula by Ono *et al.* (1978). Our interval velocity down to 2400 m shows slower velocity than that of Ono's model by 1 km/s. This is consistent with the graben-like structure that Yokoyama and Ohkawa (1986) presented.

Fig. 8 shows time sections with their folds and offset range of corresponding gathers, which correspond to the labeled step <4> in Fig. 2. Some continuous reflections appear in these sections and marked with arrows. Their two way time are consistent with those pointed in Fig. 5. Appearance of the sections matches among each other at the intersection. Short period fluctuation of the fold num-

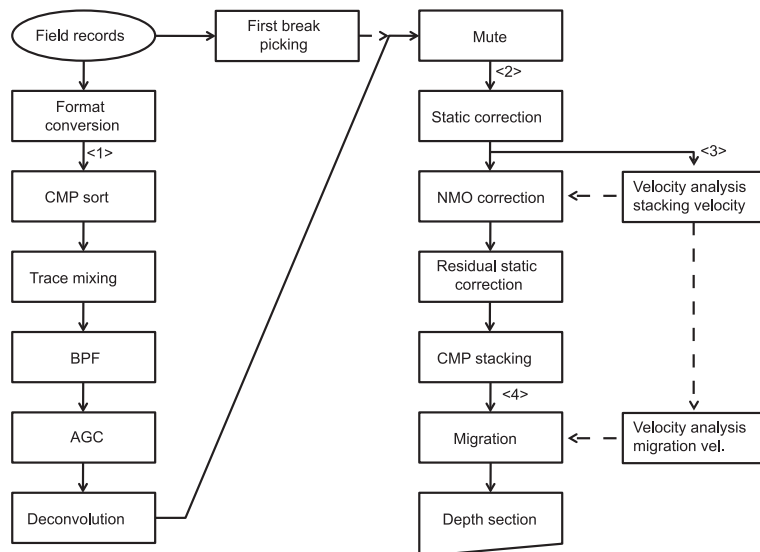


Fig. 2. The data processing. Conventional processing is included. The labels 1 to 4 are described in the text.

Table 2. The sorting parameters.

Profile	CMP spacing (m)	CMP range	length (m)	Shots
NS	23.15	0 - 219	5070	S09, S10, S11, S12
EW(W)	37.80	0 - 144	5442	S06, S11, S13, S14, S15
EW(E)	32.81	0 - 95	3116	S06, S11, S12

Datum: 372m A. S. L.

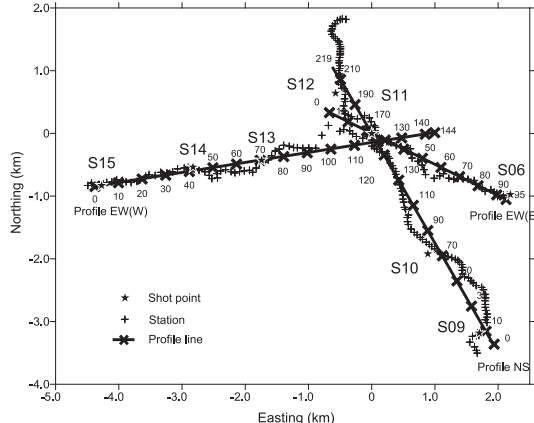


Fig. 3. Distribution of the profiles. Thick lines with the markers describe three profiles, NS, EW(W), EW (E), respectively. Numbers along the profiles are CMP location code. The crosses and stars indicate stations and shot points, respectively. The origin of the local coordinate system is the shot point S11.

ber and the offset range may cause contamination over the profiles with high frequency noise.

Then Kirchhoff depth migration (Geoltrain and Brac, 1993) was applied in order to obtain depth sections. It migrates the reflections in the apparent position to their correct location resulting improvement of spatial resolution. The simple horizontal layer model that is presented in Fig. 7b is applied. The migration aperture was 12 degree on the basis of Fresnel radius at 5.4 km in the depth of the model. The migrated sections are shown in Fig. 9.

#### 4. The final seismic sections and its interpretations

The profiles in Fig. 9 contain reflective shallow part down to ca. 5 km and less reflective deeper part. Such appearance of the profiles in Fig. 9 are similar as the seismic reflection profile by Mikada (1996) in Kirishima Volcanoes, the northern neighboring volcanoes of Sakurajima. Mikada (1996) presented a reflective upper layer above 5 km in the depth with underlying transparent layer, and a reflection horizon in the depth of 10 km.

Fig. 10 represents an interpretation of the migrated depth sections in Fig. 9. Major reflection horizons are marked as A to D. The shallower horizon A appears along

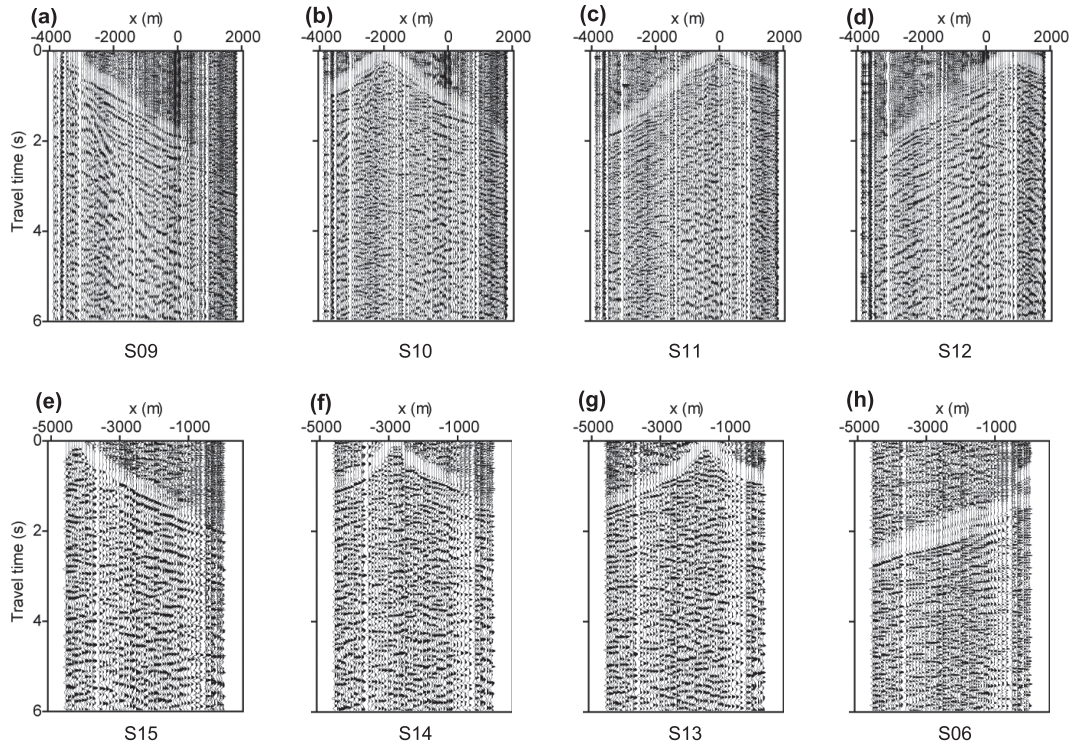


Fig. 4. Record sections. (a) for the shot S09, (b) for the shot S10, (c) for the shot S11, and (d) for the shot S12 are acquired along the profile NS. (e) for the shot S15, (f) for the shot S14, (g) for the shot S13, and (h) for the shot S06 are acquired along the profile EW(W). Horizontal axis is the location of a station. AGC (Automatic gain control) is applied on the all seismograms with 0.6s of gate time.

the line NS. The horizon A decreases its depth northward. However, the horizon A is not clear in the profiles EW(W) and EW(E). The horizon A is inferred as the horizon III of Tsutsui *et al.* (2011) and a intermediate interface in the post caldera fill on the basis of its depth and velocity around the interface (Fig. 7).

The horizon B which underlies the horizon A appears around 1800 m below the datum. Corresponding arrivals appear around 2 s in Fig. 5. The horizon B looks a pan-like interface along the line NS. The horizon appears at 1800 m below the datum at CMP 40. The horizon increases its depth gently northward. The horizon can be inferred as the “basement” in Tsutsui *et al.* (2011) on the basis of its depth. The depth of the horizon is also identical with gravity basement by Komazawa *et al.* (2008). Hence the steep rise of the horizon is acceptable at CMP 140. The horizon B is interpreted as a part of the bottom of Aira caldera for its depth and the velocity contrast (Fig. 7).

The horizon C appears flat around 5.4 km depth in all profile. The horizon C looks a boundary of reflection pattern between the continuous horizontal overlays and less continuous and undulated underlays. The horizon C can be the interface which is commonly presented in the

upper crust of south Kyushu (Ando *et al.*, 2002; Kakuta, 1982; Ono *et al.*, 1978). However, the horizon is not uniform beneath Sakurajima. The horizon C and its underlying disappear at the discontinuity H in the eastern portion of the line EW(W)(Fig. 10b).

The deepest horizon D appears on 11 km below the datum along the profiles NS and EW(W). The horizon dips northward along the profile NS. The horizon can be also the common reflector in this area because Mikada (1996) presented a reflection horizon in the same depth beneath Kirishima Volcanoes.

## 5. Discussions

### Resolution of the profiles

The migrated profiles include some artifacts which arose from heterogeneity in the folds and the offset range for small fold number analysis. We should recognize them and avoid misleading our interpretations. Following markers are shown in Fig. 10; The minimum fold boundaries are marked with thick broken lines and the offset range discontinuity are thin broken lines. Apparent weakening and apparent discontinuities of the reflection align on these broken lines.

Fresnel radius controls horizontal resolution of seismic

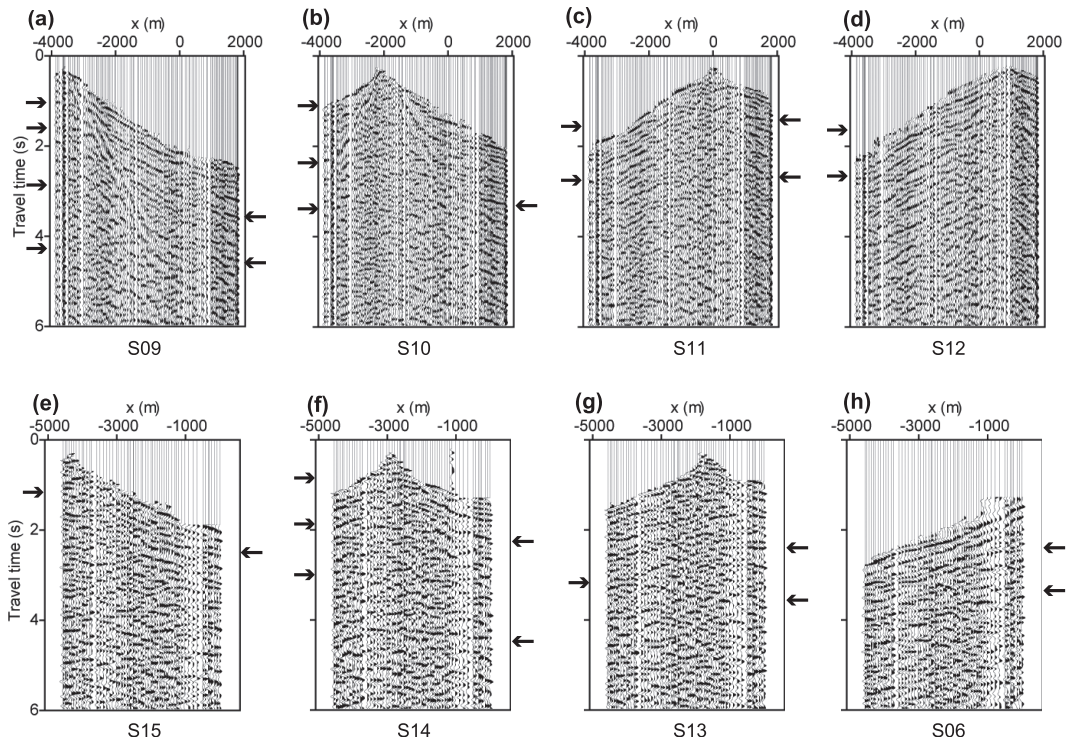


Fig. 5. Filtered, Deconvolved and muted records. The panel order is the same as the previous figure. The parameters of the deconvolution are around 0.1s as the prediction distance and 0.32s as the operation length. Arrows mark reflection arrivals and some remarkable phases. Refraction arrivals and their preceding noises are muted.

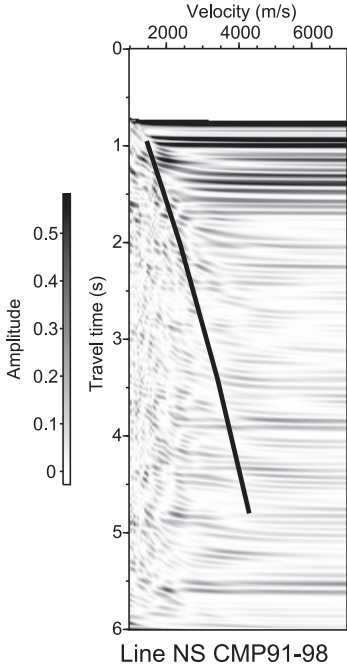


Fig. 6. An example of the velocity spectra. The spectrum is obtained on the profile NS in 2.3 to 3.6 km south of the shot S11. Gray scale represents intensity of the spectrum. A thick line represents the final velocity function. Sensitivity of velocity becomes worse with increasing two way time due to the peak broadening.

images (Yilmaz, 2001). Fig. 10d shows Fresnel radiiuses and their envelope in the same scale with the profiles. Because of poor fold number, foot-print of individual Fresnel zones which are centered at each shot point may not be cancelled out and migration noise arises at the margin of the zones. For example, some migration noise aligns along the envelope of Fresnel zone in the left end of Fig. 10a.

However the horizon D is detected in this study, it is difficult to distinguish its exact geometry, such as a point or a plane, because its extension is the same as Fresnel radius at the depth.

### The discontinuities F and H

There are two discontinuities F and H in Figs. 9 and 10. The discontinuity F spreads out around CMP 95 to 110 in the line NS (Figs. 9a and 10a). The discontinuity H appears around CMP 110 at the line EW(W) (Figs. 9b and 10b).

The discontinuity F is possibly artifact. The boundary overlays the reversed region f in 2 to 3 km below the datum. The gap e locates on the apex of the discontinuity F. The gap e arose from a lack of a shot point, and top part

of stacked seismograms beneath the gap e are distorted through the stretching in NMO processing (Fig. 8a). Therefore we concluded that the discontinuity F is a migration noise and the region f is not actual structure.

On the other hand, the discontinuity H is not an artifact. The discontinuity H looks convex face with its apex at around 5.4 km depth in the east end of the profile EW(W). Its dip angle differs from those of Fresnel envelopes and the offset range discontinuities. Hence we concluded that the discontinuity H represents a certain boundary in the actual structure.

The discontinuity H spreads out to west up to CMP 80 of the profile EW(W), and can be recognized northward from CMP160 of the profile NS. However, the discontinuity itself or any similar pattern disappear in the rest of the profiles EW(W) and NS. The discontinuity is not clear in the profile EW(E). The discontinuity H is inferred to spread out to north in the east end of the profile EW(W). Inferred distribution is mapped in Fig. 11.

The region h beneath the discontinuity H possibly represent low impedance region against the background. The low impedance is attributed to low velocity and/or low density in the region. A rapid decrease in elastic velocity is presented around the melting point of igneous rocks by Murase and McBirny (1973). And Abseth *et al.* (2005) describes impedance decrease with substitution of porous liquid into gases. One of the possible source of heat and gases is magma which is supplied from the deep part of Aira caldera and moves to Sakurajima.

The region h locates an intermediate place between the pressure source in depth at the center of caldera (Eto *et al.*, 1997) and the craters An, KDK and MDK. The depth of the discontinuity H is consistent with that of the crack top of Hidayati's model (Hidayati *et al.*, 2007).

Moreover, other geophysical studies have provided the evidences of magma beneath this area. The largest vertical displacement has been observed above the region h both in the deflation phases during 1964 to 1975 and 1988 to 1991 and in the inflation phases during 1974 to 1988 and 1991 to 1996 through the leveling surveys in the north shore of Sakurajima (Eto *et al.* 1997). Thus such the vertical displacement pattern strongly supports that magma exists in the region h.

From the above discussion, our interpretation is that the region h directly associates with magma, and that some of actual magma supply paths can locate more west than that presented by Hidayati *et al.* (2007). A chimney structure v is a possible magma supply path, which penetrates the region h. If we can have more shot points along the lines or more folds at each CMP, direct imaging of magma will be more successful.

### 6. Summary

Three seismic reflection profiles were obtained in the northeastern part of Sakurajima volcano. Four reflection

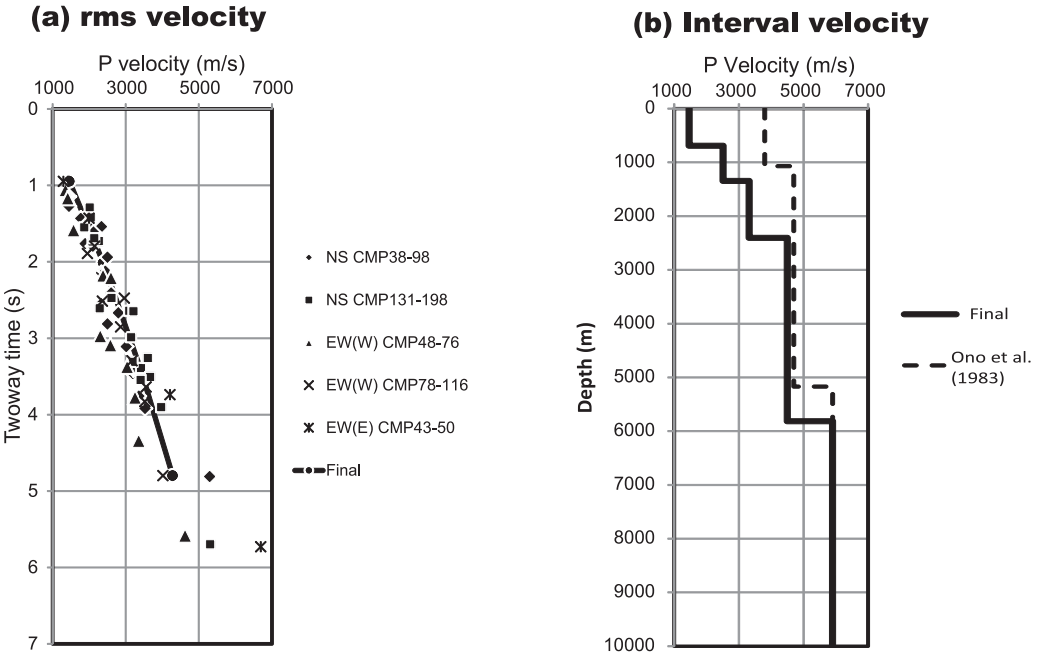


Fig. 7. Velocity structures. (a) Picked RMS velocities and the final stacking velocity function. The symbols denote picked velocities and the solid line describes the final stacking velocity. (b) Derived interval velocity. Thick solid line represents the final interval velocity derived from the final stacking velocity and broken line is the velocity model after Ono *et al.* (1978).

horizons in different depths are recognized in the depth-migrated sections. These are the horizon A around 1 km, the horizon B in 1.8 km, the horizon C around 5.4 km, and the horizon D at 11 km below the datum. The horizon A is inferred to be a reflector in post-caldera fill. The horizon B looks like a pan along the profile NS and decreases its depth westward along the profile EW(W). The horizon B corresponds with the gravity basement and inferred to be a part of floor of Aira caldera. The horizon C is the common interface in the upper crust in this area and its polarity is not uniform. The discontinuity H is found and interrupts the horizon C in the east end of the profile EW(W) and the north end of the profile NS. The depth of the discontinuity H is consistent with a top end of the preceding Hidayati's model. The underlain region h of the discontinuity H is inferred to be a low impedance which represents high temperature. The low impedance region h is interpreted to be strongly affected by magma because the largest vertical displacement has been detected above the region h. Thus it is concluded that magma supply path of Sakurajima volcano locate in more west than expected through the preceding study.

#### Acknowledgement

The data used by the present study is obtained by nice cooperation of participant (82 persons) of the 7th national project for prediction of volcanic eruption (Iguchi *et al.*, 2009) and the personnel of the Volcano Research Center, Kyoto University. Moreover, in the execution of the 2008 Project of Artificial Explosion Experiment at Sakurajima Volcano, we obtained the cooperation by local residents and organizations concerned. The colleagues of the repetitive seismic survey 2009 to 2011, Dr. Hiromitsu Oshima, Dr. Sadato Ueki, Dr. Kenji Nogami, Dr. Jun Oikawa, Dr. Takao Ohminato, Dr. Haruhisa Nakamichi, Dr. Takahiro Ohkura, Dr. Hiroshi Shimizu, and Dr. Hiroshi Yakiwara, kindly permit us to stack some part of their data at the same shot points. Moreover, the discussions with Dr. Tadashi Nishitani and Dr. Shin'ya Sakanaka in Applied geophysics laboratory, Akita-University and also with the graduates and the undergraduates were useful to compose and complete this research. Two anonymous referees gave us large amount of helpful comment to improve this manuscript. Moreover, patience of editor also encourage us. We describe all of them here and express gratitude for all of them.

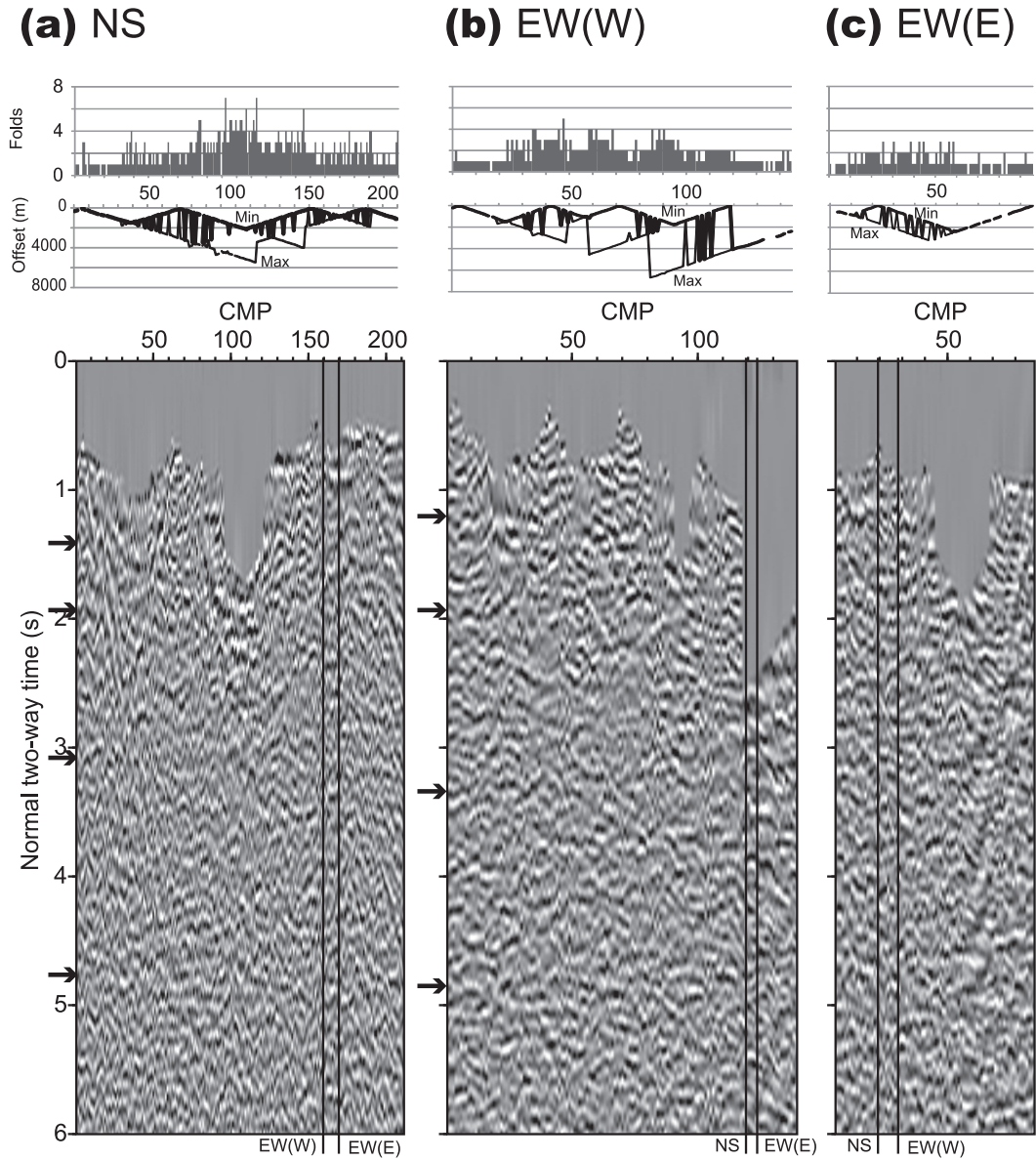


Fig. 8. Time sections. (a) The line NS, (b) the line EW(W), and (c) the line EW(E). Horizontal axes are the CMP number. The top panel represents the fold number and the middle panel is the offset range along each profile. The time section is the bottom panel. The vertical axes are the normal two way time from the datum.

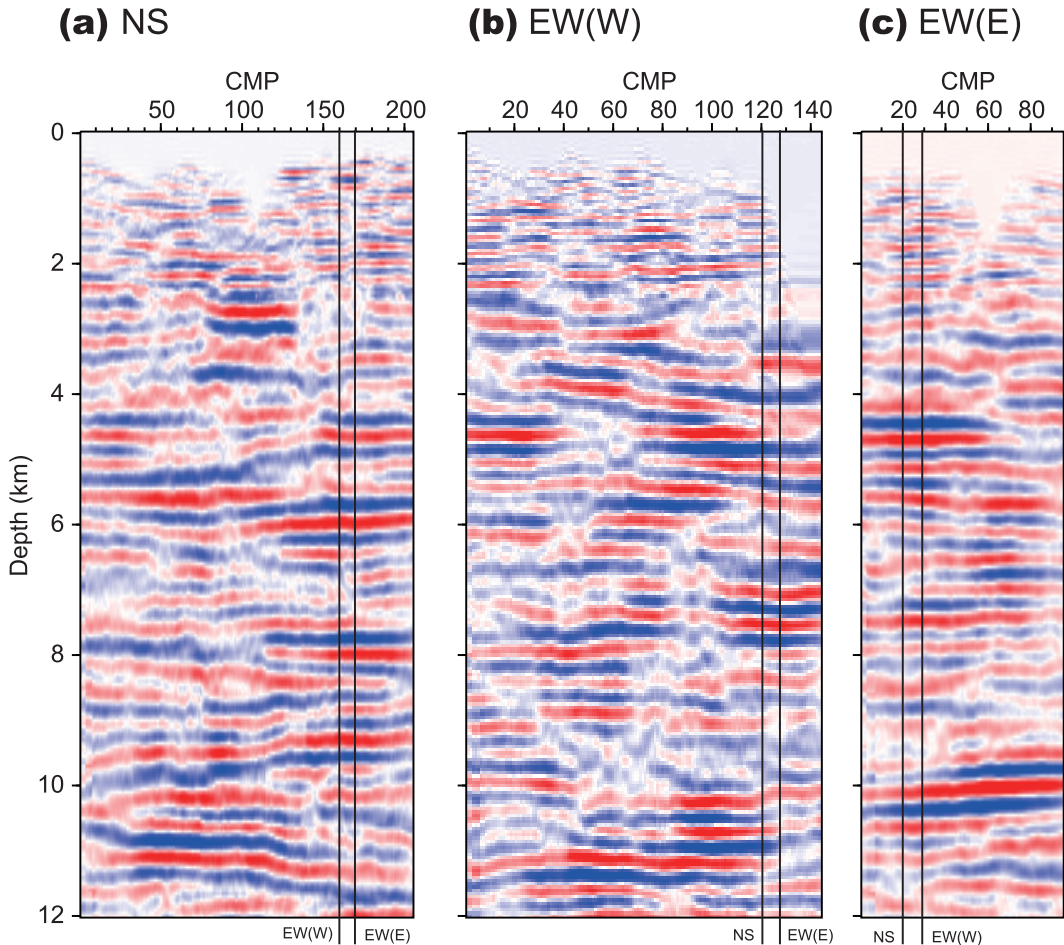


Fig. 9. Migrated depth sections. (a) The profile NS, (b) the profile EW(W), and (c) the profile EW(E). Horizontal axes are CMP number. Vertical axes are depth from the datum. Reddish color represents positive polarity and bluish color is negative polarity reflection and those densities represent intensity.

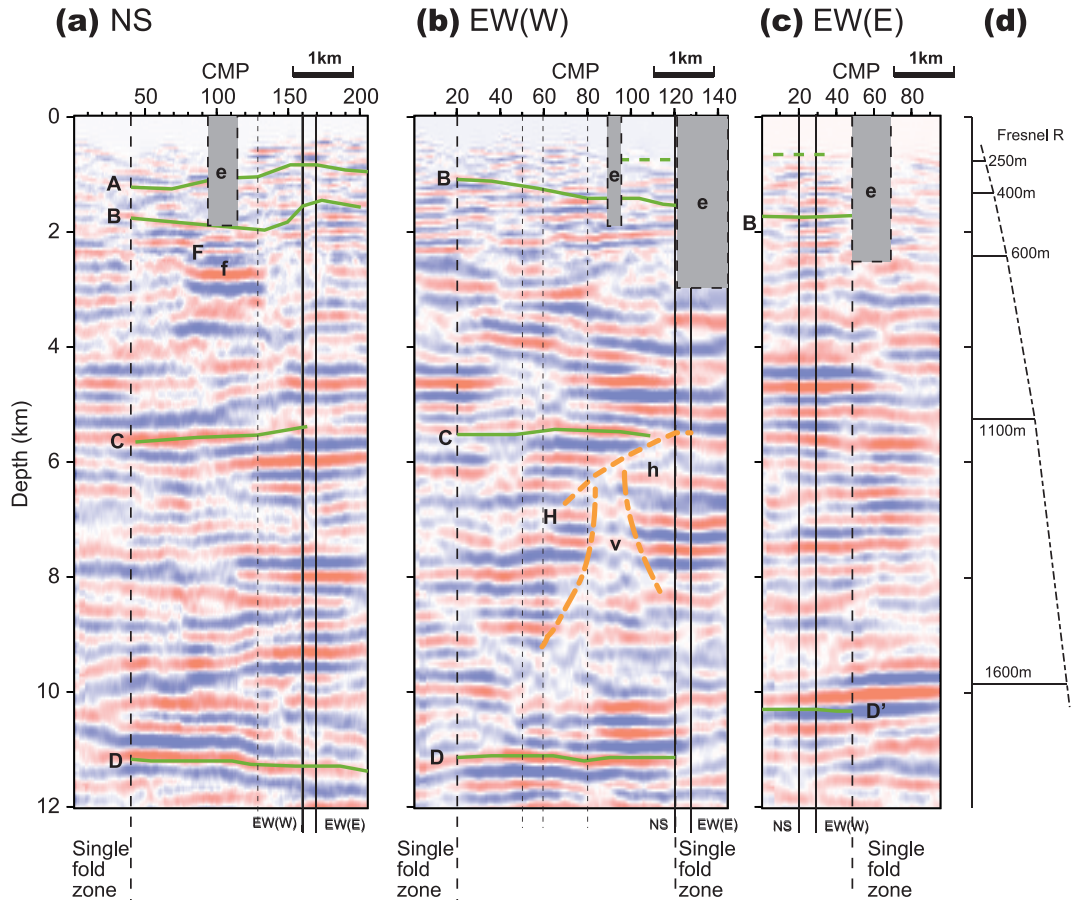


Fig. 10. Interpretation of the depth sections. (a)The profile NS, (b) the profile EW(W), (c) the profile EW(E), and (d) the corresponding Fresnel radius in depth. The zones e correspond to gaps in the time sections. The region f is considered to be artifact by the gap. Thick broken lines are boundaries of the single fold zone. Thin broken lines mark disruptions in the offset range curve (Fig. 8).

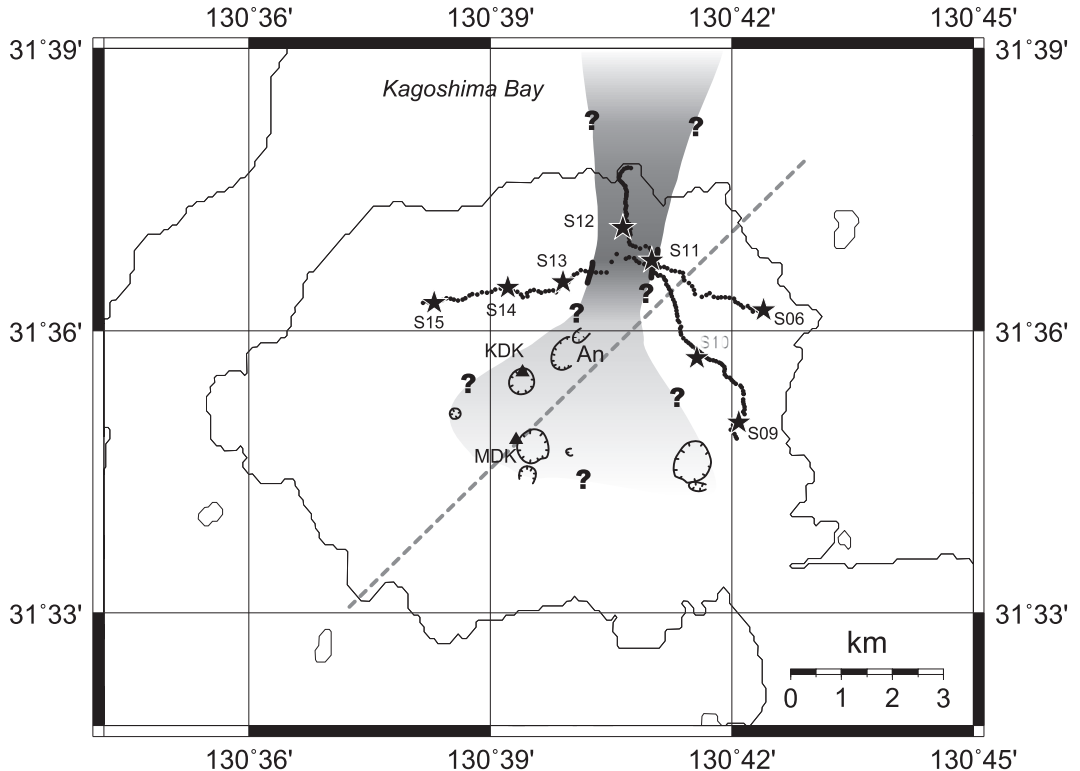


Fig. 11. Distribution of the region h. The gray zone describes a possible magma supply path which inferred through this study. The broken line represents the trace of Hidayati's model (Hidayati *et al.*, 2007). Major craters are described with hatched curves after Kobayashi (1982). "An" labels the craters of 1779–80(An-ei)'s eruption.

### References

- Ando, M., Moriya, T., Iwasaki, T., Takeda, T., Piao, C., Sakai, S., Iidaka, T., Kubo, A., Miyamachi, H., Tashiro, K., Matsushima, T., and Suzuki, S. (2002) Crustal structure beneath eastern Kyushu, Japan, derived from a wide-angle reflection and refraction experiment. *Bull. Earthq. Res. Inst. Univ. Tokyo.*, **77**, 277–285.
- Avseth, P., Mukerji, T., and Mavko, G. (2005) **Quantitative Seismic Interpretation**. Cambridge Press, 15–24.
- Cohen, J. K. and Stockwell, Jr. J. W. (2008) CWP/SU: Seismic Unix Release 41: a free package for seismic research and processing. Center for Wave Phenomena. Colorado School of Mines.
- Eto, T., Takayama, T., Yamamoto, K., Hendrasto, M., Miki, D., Sonoda, T., Matsushima, T., Uchida, K., Yakiwara, H., Wan, Y., Kimata, F., Miyazima, R., and Kobayashi, K. (1997) Re-upheaval of the ground surface at the Aira caldera, –December 1991 – October 1996-. *Annals Disast. Prev. Res. Inst., Kyoto Univ.*, **40 B-1**, 49–60 (in Japanese with English abstract).
- Fukuyama, H. and Ono, K. (1981) **Geological map of volcanoes 1 Sakurajima Volcano**. Geological Survey of Japan, 8 pp (in Japanese with English abstract).
- Geoltrain, S. and Brac, J. (1993) Can we image complex structures with first-arrival travel time?. *GEOPHYSICS*, **58**, 564–575.
- Hidayati, S., Ishihara, K. and Iguchi, M. (2007) Volcanotectonic earthquakes during the stage of magma accumulation at the Aira caldera, southern Kyushu, Japan. *Bull. Volcanol. Soc. Japan*, **52**, 289–309.
- Iguchi, M., Takayama, T., Yamazaki, T., Tada, M., Suzuki, A., Ueki, S., Ota, Y., Nakao, S., Maeno, T., Nagao, J., Baba, K., Oshige, Y., and Hoshokai, M. (2008) GPS survey in Sakurajima and around Aira caldera. In *10th Joint observation of Sakurajima volcano* (Ishihara, K. ed.), Sakurajima Volcano Research Center, Kagoshima, 53–61 (in Japanese).
- Iguchi, M., Tameguri, T. and 79 persons (2009) The 2008 Project of artificial explosion experiment at Sakurajima volcano. *Annals Disast. Prev. Res. Inst., Kyoto Univ.*, **52**, 293–307 (in Japanese with English abstract).
- Kakuta, T., (1982) Upper crustal structure in south Kyushu. *Jour. Phys. Earth*, **30**, 113–129.
- Kanda, W., Yamazaki, T., Hashimoto, T., Sakanaka, S., Yamada, K., Ogawa, Y., Aizawa, K., Takakura, S., Koyama, T., Kobayashi, S., and Komori, S. (2008) AMT

- sounding in Sakurajima volcano. In *10th Joint observation of Sakurajima volcano* (Ishihara, K. ed.), Sakurajima Volcano Research Center, Kagoshima, 89–104 (in Japanese).
- Kobayashi, T. (1982) Geology of Sakurajima volcano: a review. *Bull. Volcanol. Soc. Japan*, **27**, 277–292.
- Komazawa, M., Nakamura, K., Yamamoto, K., Iguchi, M., Akamatsu, J., Ichikawa, N., Takayama, T., and Yamazaki, T. (2008) Gravity anomalies at Sakurajima volcano, southwest Japan. *Annals Disast. Prev. Res. Inst., Kyoto Univ.*, **51B**, 261–266 (in Japanese with English abstract).
- Mikada, H. (1996) A seismic reflection analysis on refraction data from the 1994 Kirishima explosion experiment. *Kazan Bull. Volcanol. Soc. Japan*, **41**, 159–170 (in Japanese with English abstract).
- Murase T. and Mcbirney, A. R. (1973) Properties of some common igneous rocks and their melts at high temperatures. *Geol. Soc. Amer. Bull.*, **84**, 3563–3592.
- Ono, K., Ito, K., Hasegawa, I., Ichikawa, K., Iizuka, S., Kakuta, T. and Suzuki, H. (1978) Explosion seismic studies in south Kyushu especially around the Sakurajima volcano. *J. Phys. Earth*, **26**, 309–319.
- Tsutsui, T., Imai, M., Tsushima, K., Yagi, N., Iguchi, M. and Tameguri, T. (2011) The shallow structure imaging in the northeastern part of the Sakurajima volcano with the pseudo-reflection method. *Bull. Volcanol. Soc. Japan*, **56**, 201–212 (in Japanese with English abstract).
- Yagi, N. and Tsutsui, T. (2009) An introduction guide to Seismic Un\*x (SU) for Mac OS X 10. 5 (Leopard) users. *Butsuri-Tansa*, **62**, 361–368 (in Japanese with English abstract).
- Yokoyama, I. and Ohkawa, S. (1986) The subsurface structure of the Aira caldera and its vicinity in southern Kyushu. *Japan. J. Volcanol. Geotherm. Res.*, **30**, 253–282.
- Yilmaz, O. (2001) **Seismic Data Analysis** Vol. 1. Society of Exploration Geophysicist, 1000 pp.  
 (Editorial handling Yosuke Aoki)

## 桜島火山北東部の地震反射構造

筒井智樹・八木直史・井口正人・為栗 健・三ヶ田 均・  
 尾西恭亮・宮町宏樹・西村太志・森田裕一・渡邊篤志

桜島火山で反射法地震探査を行い深さ 11 km までの 3 つの反射断面を得た。2 本の地震探査測線は 221 点の臨時観測点と 8 点の発振点で構成された。1 本の測線は桜島の東麓に展開され、もう 1 本の測線は桜島の北山腹に展開された。これらのデータに通常の反射法地震探査の処理を行い、深度マイグレーションを施して深度断面を得た。得られた反射断面には 4 つの連続した反射面が認められる。このうち深さ 5.4 km 付近の反射面は桜島北東部で消失する。この反射面の不連続の下にはマグマかその供給経路が存在する可能性が高い。桜島のマグマ供給経路は先行研究のモデルより西側に位置している可能性がある。